



The efficacy of receptor tyrosine kinase EphA2 autophosphorylation increases with EphA2 oligomer size

Received for publication, May 4, 2022, and in revised form, August 9, 2022. Published, Papers in Press, August 13, 2022.
<https://doi.org/10.1016/j.jbc.2022.102370>

Elmer Zapata-Mercado¹, Gabriel Biener², Daniel M. McKenzie¹, William C. Wimley³, Elena B. Pasquale^{4,*}, Valerica Raicu^{2,5,*}, and Kalina Hristova^{1,*}

From the ¹Department of Materials Science and Engineering, Johns Hopkins University, Baltimore, Maryland, USA; ²Department of Physics, University of Wisconsin, Milwaukee, Wisconsin, USA; ³Tulane University School of Medicine, Department of Biochemistry and Molecular Biology, New Orleans, Louisiana, USA; ⁴Cancer Center, Sanford Burnham Prebys Medical Discovery Institute, La Jolla, California, USA; ⁵Department of Biological Sciences, University of Wisconsin, Milwaukee, Wisconsin, USA

Edited by Wolfgang Peti

The receptor tyrosine kinase (RTK) EphA2 is expressed in epithelial and endothelial cells and controls the assembly of cell–cell junctions. EphA2 has also been implicated in many diseases, including cancer. Unlike most RTKs, which signal predominantly as dimers, EphA2 readily forms high-order oligomers upon ligand binding. Here, we investigated if a correlation exists between EphA2 signaling properties and the size of the EphA2 oligomers induced by multiple ligands, including the widely used ephrinA1-Fc ligand, the soluble monomeric m-ephrinA1, and novel engineered peptide ligands. We used fluorescence intensity fluctuation (FIF) spectrometry to characterize the EphA2 oligomer populations induced by the different ligands. Interestingly, we found that different monomeric and dimeric ligands induce EphA2 oligomers with widely different size distributions. Our comparison of FIF brightness distribution parameters and EphA2 signaling parameters reveals that the efficacy of EphA2 phosphorylation on tyrosine 588, an autophosphorylation response contributing to EphA2 activation, correlates with EphA2 mean oligomer size. However, we found that other characteristics, such as the efficacy of AKT inhibition and ligand bias coefficients, appear to be independent of EphA2 oligomer size. Taken together, this work highlights the utility of FIF in RTK signaling research and demonstrates a quantitative correlation between the architecture of EphA2 signaling complexes and signaling features.

Assessment of oligomer sizes of membrane protein complexes in live cells poses unique challenges, as most methods used for soluble proteins are not applicable in the context of the native plasma membrane. Fluorescence-based methods are often the only option available to probe the oligomerization of membrane proteins suitably labeled with fluorophores. Widely used fluorescent-based techniques are FRET, fluorescence lifetime imaging, and fluorescence fluctuation spectroscopy (1–6). Of those, the fluorescence fluctuation techniques are uniquely suited to directly assess oligomer size, which is

proportional to the molecular brightness measured (7–9). Some of these fluorescence fluctuation methods are based on fluorescence cross-correlation spectroscopy (FCCS), a technique in which the dynamics, concentration, and interactions of diffusing proteins labeled with a fluorophore are determined by spatial autocorrelation analysis (10). FCCS often utilizes pulsed interleaved excitation *via* two synchronized lasers with a time delay between them, such that the energy transfer to the acceptor and the direct excitation of the acceptor are separated in time (11). Pulsed interleaf excitation–FCCS has been used to study the interactions of proteins in cellular membranes (12–14), but its implementation requires specialized equipment capable of single-molecule fluorescence measurements (11).

An example of a technique that measures fluorescence fluctuation on a standard confocal microscope is number and brightness (N&B) (15–17). N&B works by rapidly acquiring a stack of images of the same region of a cell and then computing the mean fluorescence intensity and the variance of the intensity across the stack for each pixel. The molecular brightness, defined as the ratio of the variance of the fluorescence intensity over time to the mean fluorescence intensity, is known to scale with the oligomer size. The average oligomer size is then easily calculated by normalizing the molecular brightness measured for a protein of interest to the molecular brightness of a monomer control. However, a caveat is that a large immobile oligomer would be invisible in N&B analysis, as no fluctuations would arise over time.

While N&B monitors fluorescence fluctuations over time, other techniques such as spatial intensity distribution analysis (SPIDA) quantify fluctuations over space (18). SPIDA works by generating histograms of pixel fluorescence intensities from a region of interest (ROI) in the cell membrane to calculate molecular brightness for this region; brightness values from several such regions are used to calculate the average size of the oligomers in the sample. Recently, a space-based intensity analysis method similar to SPIDA and termed “fluorescence intensity fluctuation (FIF) spectrometry” was introduced, which is particularly well suited for heterogeneous populations of oligomers (8). FIF spectrometry calculates the molecular

* For correspondence: Kalina Hristova, kh@jhu.edu; Elena B. Pasquale, elenap@sbsdsccovery.org; Valerica Raicu, vraicu@uwm.edu.

EphA2 phosphorylation correlates with EphA2 oligomer size

brightness of fluorescent protein–tagged receptors in small segments of the plasma membrane and creates a histogram of these molecular brightness values derived from thousands of such segments. Here, we explore the utility of FIF in studies of EphA2 association in the plasma membrane.

The EphA2 receptor is highly expressed in epithelial and endothelial cells, where it triggers diverse downstream signaling pathways that control the assembly of cell–cell junctions. This receptor has been implicated in many physiological and disease processes, such as cancer (19–21), pathological angiogenesis (22–26), inflammation (22, 27–29), cataracts (30–33), psoriasis (34), and parasite infections (20, 35). In many cases, ligand-induced EphA2 signaling has been recognized as antioncogenic, and thus agents that activate EphA2 could be useful as cancer therapeutics (36).

EphA2 belongs to the receptor tyrosine kinase (RTK) family. It is a single-pass transmembrane receptor with an extracellular region that binds the activating ligands (ephrins) and an intracellular region that contains the tyrosine kinase domain. The kinase domain is activated by autophosphorylation of tyrosine residues occurring upon close contact of neighboring EphA2 molecules. Therefore, lateral interactions of EphA2 molecules are the first required step in EphA2 signal transduction in the plasma membrane.

While most of the 58 RTKs signal mainly as dimers, EphA2, in addition, can form high-order oligomers (37–41). Published work has suggested that the size of the oligomers may affect signaling function. For instance, ephrinA1 immobilized on artificial lipid bilayers or nanocalipers can cause different EphA2 signaling responses depending on the size of the EphA2 oligomers induced (42, 43). However, the exact functional dependence of EphA2 signaling on the oligomerization state of the receptor is unknown. Challenges that have plagued such investigations have been (1) limited ability to control the oligomer size of EphA2 assemblies in cells and (2) limited methods to quantify heterogeneous distributions of oligomer sizes for membrane receptors. In this study, we overcome these limitations to investigate if a correlation exists between EphA2 oligomer size and signaling properties.

This work was empowered by the recent discovery of a series of small engineered peptides that bind specifically to EphA2 and activate it (40). The peptides used here are either monomers (YSA, YSA-bio, with biotin attached to the C terminus, or monomer 10, which also has biotin at the C terminus) or constitutive dimers. These peptides bind to the broad and shallow ephrin-binding pocket in the extracellular region of EphA2, which is easily accessible on the cell surface (44–50). The engineered peptides have been designed to modulate the association of EphA2 molecules (40) and thus potentially modulate EphA2 oligomer size.

The different dimeric peptide ligands used in this study have different potencies and different efficacies, depending on their sequence and configuration (40). These dimeric peptides are highly selective, and some of them have been shown to stimulate EphA2 signaling responses with unprecedented subnanomolar potency (40). Furthermore, the peptides and the monomeric soluble form of the ephrinA1 ligand (m-ephrinA1)

have been shown to induce biased signaling compared with the widely used ligand ephrinA1-Fc, which consists of the ephrinA1 extracellular region dimerized by fusion to the Fc portion of an antibody (40). In particular, these ligands can differentially modulate two EphA2 signaling responses: EphA2 autophosphorylation on tyrosine 588 (Y588, a site in the juxtamembrane segment whose phosphorylation promotes EphA2 kinase activity and activation of downstream signaling) and inhibition of AKT phosphorylation on serine 473 (a site critical for AKT activation) (51, 52).

The dimeric peptide ligands have been engineered from monomeric precursors through N-terminal, C-terminal, or N–C-terminal linkages (40). Based on molecular modeling, we previously hypothesized that these dimeric peptides stabilize different types of EphA2 dimers, engaging different interfaces and perhaps exhibiting different signaling properties (40). However, we found that all the dimeric peptides induce the formation of EphA2 oligomers. Using mutagenesis of two crystallographic extracellular interfaces, the “dimerization” interface and the “clustering” interface (38), we showed that a C-terminally linked dimeric peptide induces EphA2 oligomers that utilize both interfaces (40). In contrast, an N-terminally linked dimeric peptide induces EphA2 oligomers that utilize the dimerization but not the clustering interface (40). Here, we investigate differences in the size of EphA2 oligomers that form in response to ephrinA1-Fc, m-ephrinA1, three monomeric peptide ligands, and three dimeric peptide ligands with different configurations (40).

Results

FIF spectrometry

We sought to assess the oligomerization state of EphA2, labeled with enhanced YFP (eYFP), using FIF spectrometry (8). Attachment of eYFP to the C terminus of EphA2 *via* a 15 amino acid (GGS)₅ flexible linker has been previously shown to not affect EphA2 autophosphorylation (53). Following EphA2-eYFP expression in transiently transfected human embryonic kidney 293T (HEK293T) cells without ligand treatment (Fig. 1A) or treated with different ligands (Fig. 1B), the plasma membrane in contact with the substrate was imaged by confocal microscopy as previously described (54). We observed that the plasma membrane exhibits homogeneous EphA2-eYFP fluorescence in the absence of ligands (Fig. 1A). However, upon ligand addition, heterogeneities appear within a minute or two (Fig. 1B). The appearance of such “puncta” of EphA2 fluorescence in response to ligand binding has been reported in the literature (40, 55) and used to determine whether EphA2 mutations affect receptor functionality (39). Interestingly, the appearance of the puncta is characteristically distinct for the different ligands (Fig. 1B).

Fluorescence micrographs including ~200 to 300 cells were analyzed with the FIF spectrometry software (8). In the first step of the analysis, a selected area of the plasma membrane (Fig. 1A, P1) is divided into smaller segments with a preset size (15 × 15 pixels; Fig. 1A, P2). Next, the distribution of the 225 pixel-level intensity values in each segment is fit with a

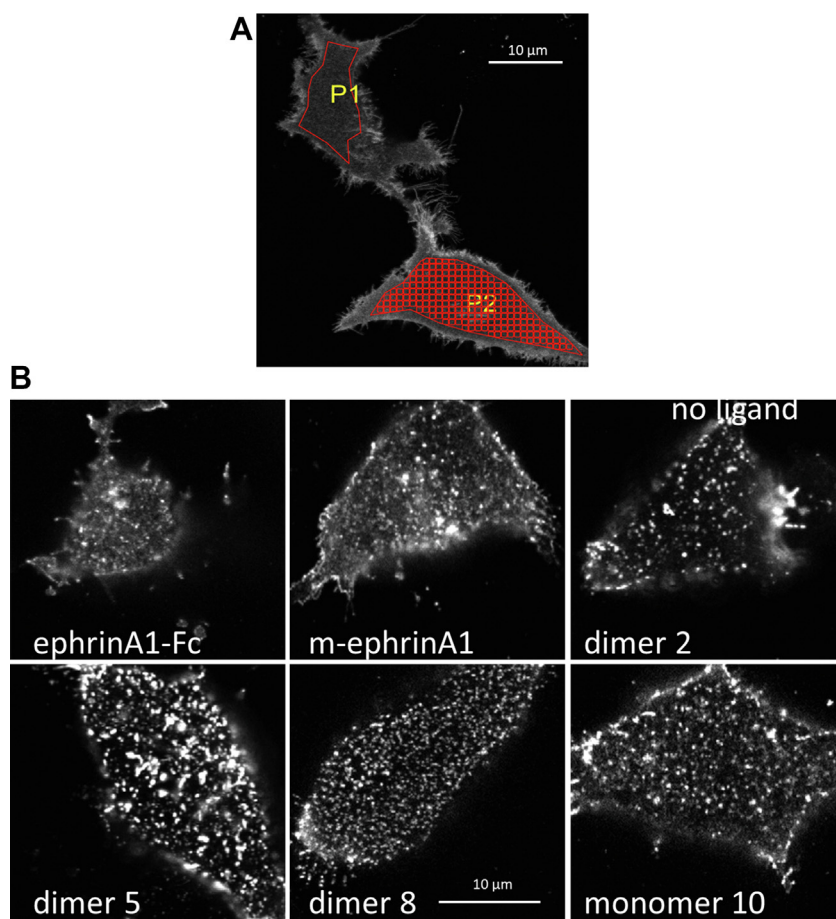


Figure 1. Confocal images of plasma membranes facing the solid support. HEK293T cells were transiently transfected with a plasmid encoding EphA2-eYFP. *A*, no ligand stimulation. An area of the plasma membrane is selected (P1, red outline) and then segmented for FIF analysis (P2, red grid) to determine the molecular brightness in each 15×15 pixel segment. *B*, cells stimulated with the indicated ligands at saturating concentrations (Table 1). eYFP, enhanced YFP; HEK293T, human embryonic kidney 293T cell line.

Gaussian function, yielding for each segment the mean ($\langle I_{\text{segment}} \rangle$) and the width (σ_{segment}) of the fitted Gaussian. The variance ($\sigma_{\text{segment}}^2$) and $\langle I_{\text{segment}} \rangle$ are then used to calculate the molecular brightness in each segment of the plasma membrane ($\epsilon_{\text{segment}}$) according to Equation 1 in the [Experimental procedures](#) section. Finally, the brightness values from thousands of segments are histogrammed to yield molecular brightness distributions (8).

The brightness distribution for EphA2 in the absence of ligand is shown in Figure 2A, along with the measured brightness distribution of the monomeric control LAT (linker for activation of T cells) (6, 17) and the dimeric control TrkA in cells treated with nerve growth factor (NGF) (54). The distributions are scaled by integrating the curves and normalizing the amplitudes so that the area under the curve is the same for the three proteins. The EphA2 brightness distribution is between the brightness distributions of the monomer and dimer controls, indicating that EphA2 exists in a monomer/dimer equilibrium when a ligand is not present. This conclusion is in agreement with prior FRET studies (37, 41).

Next, we performed FIF experiments in the presence of different ligands. The ligands were used at concentrations

that greatly exceed their measured dissociation constants and/or their potency (EC_{50}) for EphA2 Y588 phosphorylation in cells, so that most EphA2 molecules are ligand bound (Table 1). Once all the binding sites on the EphA2 receptors are occupied, Y588 phosphorylation is the same irrespective of ligand concentrations. The brightness distributions in the presence of the ligands are compared with the brightness distribution of the TrkA + NGF dimer control (54) (Fig. 2B). All the brightness distributions were scaled so that the area under the curve is the same, allowing direct comparisons. We observed that most of the ligands shifted the distributions of brightness to higher values, indicative of the induction of high-order oligomers that are larger than dimers. In contrast, the EphA2 brightness distribution in the presence of one of the ligands, the YSA peptide, is very similar to that of TrkA + NGF (Fig. 2B), indicating that YSA induces the formation of EphA2 dimers rather than high-order oligomers. There are also differences among the other ligands, suggesting differences in the size of the oligomers induced. For example, the brightness distribution in response to treatment with monomer 10 is the least shifted to higher brightness values, and the distribution for dimer 8 is the most shifted.

EphA2 phosphorylation correlates with EphA2 oligomer size

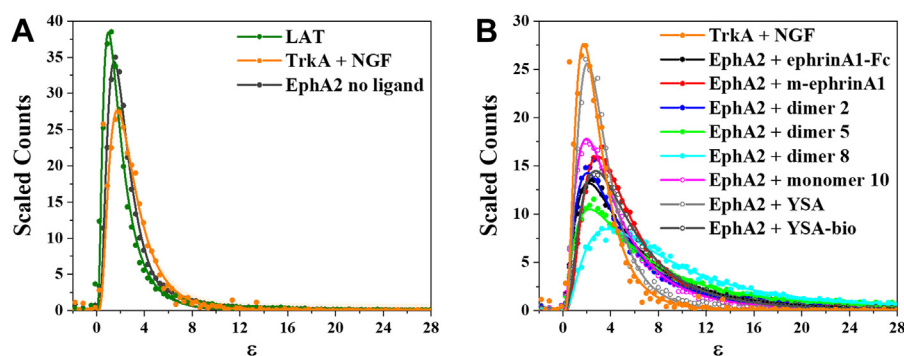


Figure 2. EphA2-eYFP molecular brightness distributions. A, molecular brightness (ϵ) distributions for EphA2-eYFP in the absence of ligand, LAT (monomer control), and TrkA + NGF (dimer control), where all three distributions are normalized to the same area under the curve. The EphA2 molecular brightness distribution in the absence of ligand is between the monomer and dimer controls, indicating that EphA2 exists predominantly in a monomer-dimer equilibrium. B, molecular brightness distributions for EphA2 in the presence of the indicated ligands, compared with the brightness distribution measured for TrkA + NGF. The distribution in the presence of YSA is similar to the TrkA + NGF dimer control, whereas the distributions for the other ligands are shifted to higher brightness values. LAT, linker for activation of T cells; NGF, nerve growth factor.

All distributions are well described by log-normal functions (see Equation 2 in the [Experimental procedures](#) section). The two best-fit parameters of the respective normal $\ln(\text{brightness})$ distributions (mean μ and standard deviation σ) were used in Equations 3–5 to calculate the three characteristic parameters of the log-normal distributions: mean (the average brightness), median (the middle of the sorted brightness values), and mode (the position of the maximum of the distribution) (Table 2).

Correlations between EphA2 signaling parameters and brightness distributions

To determine if EphA2 signaling properties correlate with the parameters of the brightness distributions, we plotted previously determined parameters that describe EphA2 signaling (40) as a function of the mean, median, and mode of the log-normal brightness distributions (Figs. 3, S1 and S2, and Table S1). The EphA2 signaling parameters we considered include (A) ligand bias coefficients (β_{lig}), which describe the ability of the different ligands to inhibit AKT serine 473 phosphorylation as compared with increasing EphA2 Y588 phosphorylation; (B) ligand-specific efficacy of EphA2 phosphorylation on Y588 (E_{top} pY588); (C) ligand-specific efficacy of inhibition of AKT phosphorylation (E_{top} pAKT_{inh}), a well-known EphA2 downstream signaling response; and (D)

ligand-specific ratios of Y588 phosphorylation to AKT inhibition potencies (EC_{50} pY588/ EC_{50} pAKT_{inh}).

Quantification of bias involves the calculation of a single numerical value (a bias coefficient β_{lig}) for each ligand, which reports on the existence and magnitude of ligand bias (56, 57). The ratio of the two fitted parameters, E_{top}/EC_{50} , has been recognized as an important descriptor of ligand activity (58), and ligand bias coefficients can be calculated using these ratios for different ligands and responses. The bias coefficients β_{lig} for the peptide ligands and m-ephrinA1 have revealed that these ligands significantly bias signaling toward inhibiting AKT *versus* promoting EphA2 Y588 phosphorylation, as compared with ephrinA1-Fc (40). The bias coefficients for the peptide ligands and m-ephrinA1 are similar, yet the mean brightness values for these ligands are very different (Fig. 3A). Furthermore, ephrinA1-Fc exhibits an intermediate brightness value. Thus, there appears to be no correlation between bias coefficients and mean brightness. This was confirmed by fitting a linear function to the peptide and m-ephrinA1 β_{lig} values (Fig. 3A), and determining whether a significant correlation is present by comparing the slope to the null hypothesis of 0 slope (corresponding to no correlation) using a one-sample *t* test. The *p* value obtained confirms that there is no correlation (Table S1). In contrast, EphA2 Y588 phosphorylation efficacy appears to increase as a function of mean

Table 1
EphA2 ligands used

Ligand	Sequence	K_d (nM)	EC_{50} , pY588 (nM)	[L] (nM)
ephrinA1-Fc		ND	3.8 ± 0.2	50
m-ephrinA1		20–30 (68)	74 ± 6	200
Dimer 2	β AWLAYPDSVPYRPKC β AWLAYPDSVPYRPKC	380 ± 80 (40)	5.6 ± 0.6	1200
Dimer 5	CGWLAYPDSVPYRPK CGWLAYPDSVPYRPK	21 ± 3 (40)	0.75 ± 0.07	1500
Dimer 8	β AWLAYPDSVPYRPKG- -GAWLAYPDSVPYRPKam	ND	0.73 ± 0.06	2000
Monomer 10	CcamGAWLAYPDSVPYRPK-bio	80 ± 21 (40)	180 ± 20	6300
YSA	YSAYPDSVPMMMSGSGSK	8000 ± 1700 (45)	ND	50,000
YSA-bio	YSAYPDSVPMMMSGSGSK-bio	9800 ± 0 (45)	3900 ± 380	50,000

Abbreviation: ND, not determined.

K_d is the dissociation constant as reported (40, 45, 68), and [L] is the ligand concentration used in the FIF experiments. Here, we use concentrations that exceed the measured dissociation constants and the EC_{50} in dose-response curves.

Table 2
Parameters of the molecular brightness log-normal distributions

Whole membrane	μ	σ	Mean	Median	Mode
LAT	0.49 ± 0.02	0.71 ± 0.01	2.10 ± 0.04	1.63 ± 0.03	1.00 ± 0.03
TrkA + NGF	0.94 ± 0.01	0.62 ± 0.01	3.10 ± 0.03	2.56 ± 0.02	1.74 ± 0.02
No ligand	0.74 ± 0.01	0.60 ± 0.01	2.52 ± 0.02	2.10 ± 0.01	1.47 ± 0.01
ephrinA1-Fc	1.57 ± 0.01	0.89 ± 0.01	7.17 ± 0.09	4.81 ± 0.05	2.16 ± 0.04
m-ephrinA1	1.51 ± 0.01	0.66 ± 0.004	5.60 ± 0.03	4.51 ± 0.02	2.91 ± 0.02
Dimer 2	1.45 ± 0.01	0.85 ± 0.01	6.12 ± 0.09	4.26 ± 0.05	2.06 ± 0.04
Dimer 5	1.81 ± 0.01	1.00 ± 0.01	10.02 ± 0.16	6.08 ± 0.08	2.24 ± 0.05
Dimer 8	2.08 ± 0.01	0.87 ± 0.01	11.66 ± 0.16	8.00 ± 0.09	3.77 ± 0.07
Monomer 10	1.33 ± 0.01	0.80 ± 0.01	5.22 ± 0.05	3.78 ± 0.03	1.98 ± 0.02
YSA	1.08 ± 0.01	0.59 ± 0.01	3.52 ± 0.03	2.95 ± 0.02	2.07 ± 0.02
YSA-bio	1.55 ± 0.01	0.74 ± 0.01	6.20 ± 0.05	4.73 ± 0.03	2.74 ± 0.02

The mean, median, and mode of the log-normal distributions are calculated according to Equations (3), (4), and (5), respectively. μ and σ are the two best-fit parameters of the respective $\ln(\text{brightness})$ normal distributions (Equation 2).

brightness (Fig. 3B). To determine if a correlation exists in this case, we fit a linear function to the data points for m-ephrinA1 and the peptide ligands, again excluding ephrinA1-Fc. Comparing the slope to the null hypothesis of 0 slope yielded a p value <0.01, which is indicative of a significant correlation (Table S1). Similar analyses for the efficacies of inhibition of AKT phosphorylation (Fig. 3C) and the ratios of the potencies of Y588 phosphorylation to AKT inhibition (Fig. 3D) show no correlation (Table S1).

Analyses for the median (Fig. S1) and mode (Fig. S2) of the molecular brightness distributions only revealed one additional significant correlation, which shows that the efficacy of

EphA2 Y588 phosphorylation increases with the increase in median molecular brightness (Table S1).

Molecular brightness in EphA2-eYFP puncta

To determine whether the ligand-induced increased brightness in the puncta (Fig. 1B) might reflect the presence of larger EphA2 oligomers (39), we investigated EphA2 oligomer sizes in the puncta using FIF. Notably, FIF spectrometry can inherently filter out information about the brighter puncta because FIF data processing can ignore membrane inhomogeneities with anomalously high intensities within a

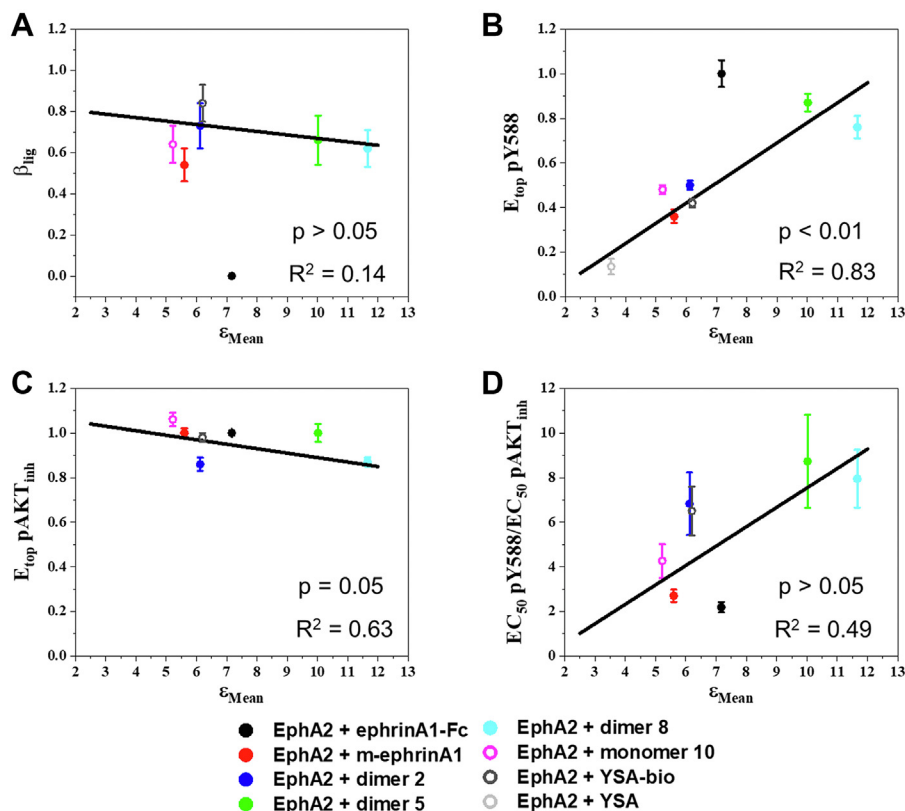


Figure 3. Correlation between EphA2 signaling parameters and the means of the molecular brightness log-normal distributions obtained from FIF analysis of whole membranes. A, ligand bias coefficients versus means, when ephrinA1-Fc was used as the reference ligand. B, ligand-specific EphA2 Y588 phosphorylation efficacies, normalized to the value obtained with the reference ligand ephrinA1-Fc, versus the means. C, ligand-specific AKT inhibition efficacies, normalized to the value obtained with the reference ligand ephrinA1-Fc, versus means. D, ligand-specific ratios of Y588 phosphorylation to AKT inhibition potencies versus means. Data points: averages and standard errors from (40). Lines: linear fits, excluding ephrinA1-Fc. EphA2 + YSA only shown in B. FIF, fluorescence intensity fluctuation.

EphA2 phosphorylation correlates with EphA2 oligomer size

segment and fit with Gaussian functions mainly the low-intensity portion of the intensity distributions (8). This can reduce the contributions of the high-intensity pixels to the calculated mean and variance in each segment. Thus, the standard FIF analyses performed previously may filter out some information about the puncta.

To specifically analyze the pixels in the puncta, we used a recent augmentation of the FIF method (9). In the first step of the augmented method, segments are subjected to a simple linear iterative clustering (SLIC) algorithm that identifies puncta and separates them from the cell membrane images for further analysis (9). Figure 4A shows an example of cell images after removal of the pixels identified as belonging to puncta. Since the puncta are typically too small for reliable FIF analysis, in the second step of the augmented method, the pixel content of at least four puncta with similar average intensities is combined into clusters, yielding a single molecular

brightness value for each cluster. Brightness values derived from the clusters of puncta are then histogrammed in the third step and analyzed as described previously for whole membranes. This algorithm has been previously used (9), and it has been argued that the inherent property of FIF to filter out extreme intensity values makes whole membrane analyses essentially equivalent to analyses of membranes from which puncta are removed by the algorithm.

Analysis of the EphA2 puncta revealed that the brightness distributions for all the ligands are shifted to higher brightness as compared with whole membranes (Fig. 4B compared with Fig. 2B). Comparison of the EphA2 concentrations obtained from the whole membrane and puncta analyses shows average concentrations approximately three times higher in the puncta (Fig. 5). However, the concentration distributions are broad, consistent with the fact that EphA2 was introduced *via* transient transfection.

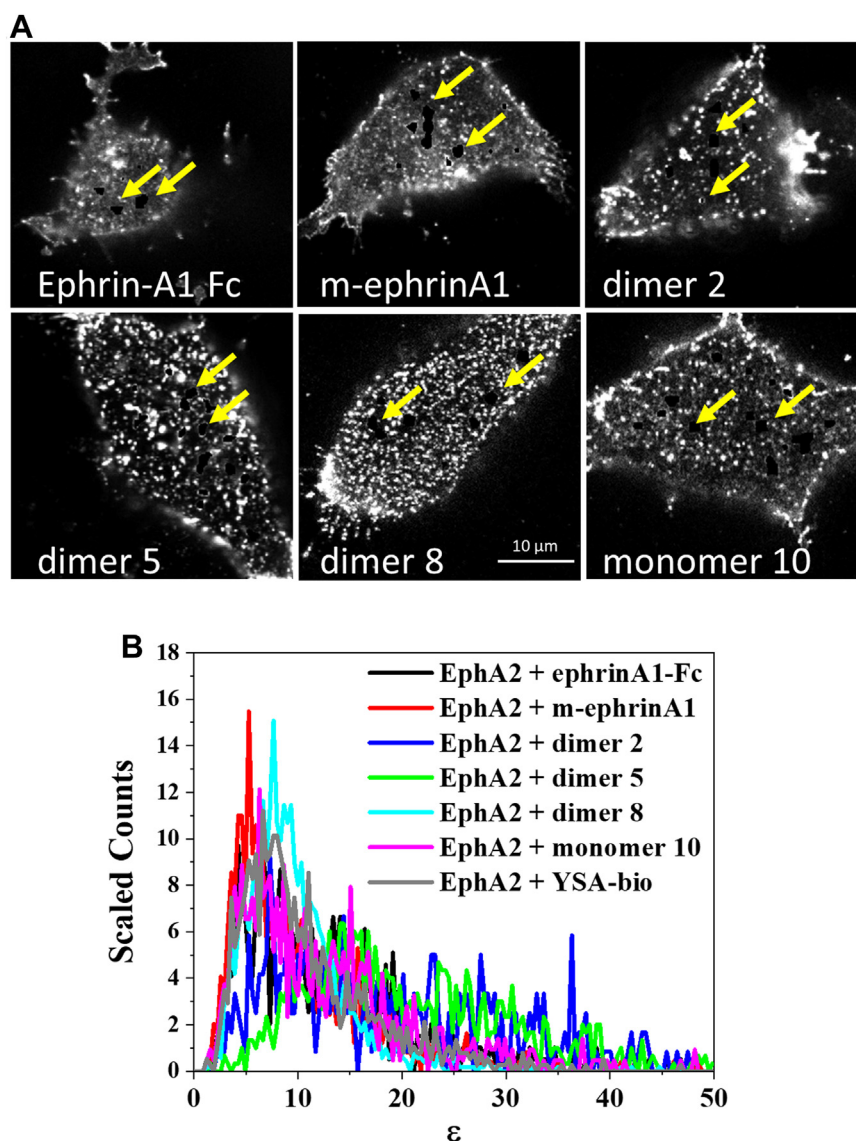


Figure 4. FIF analysis of EphA2-eYFP puncta. A, the cells in Figure 1B, with some puncta removed using the SLIC algorithm (as indicated by the yellow arrows). B, molecular brightness distributions for high-intensity EphA2 puncta in the presence of the indicated ligands, normalized to the same area under the curve. FIF, fluorescence intensity fluctuation; SLIC, simple linear iterative clustering.

EphA2 phosphorylation correlates with EphA2 oligomer size

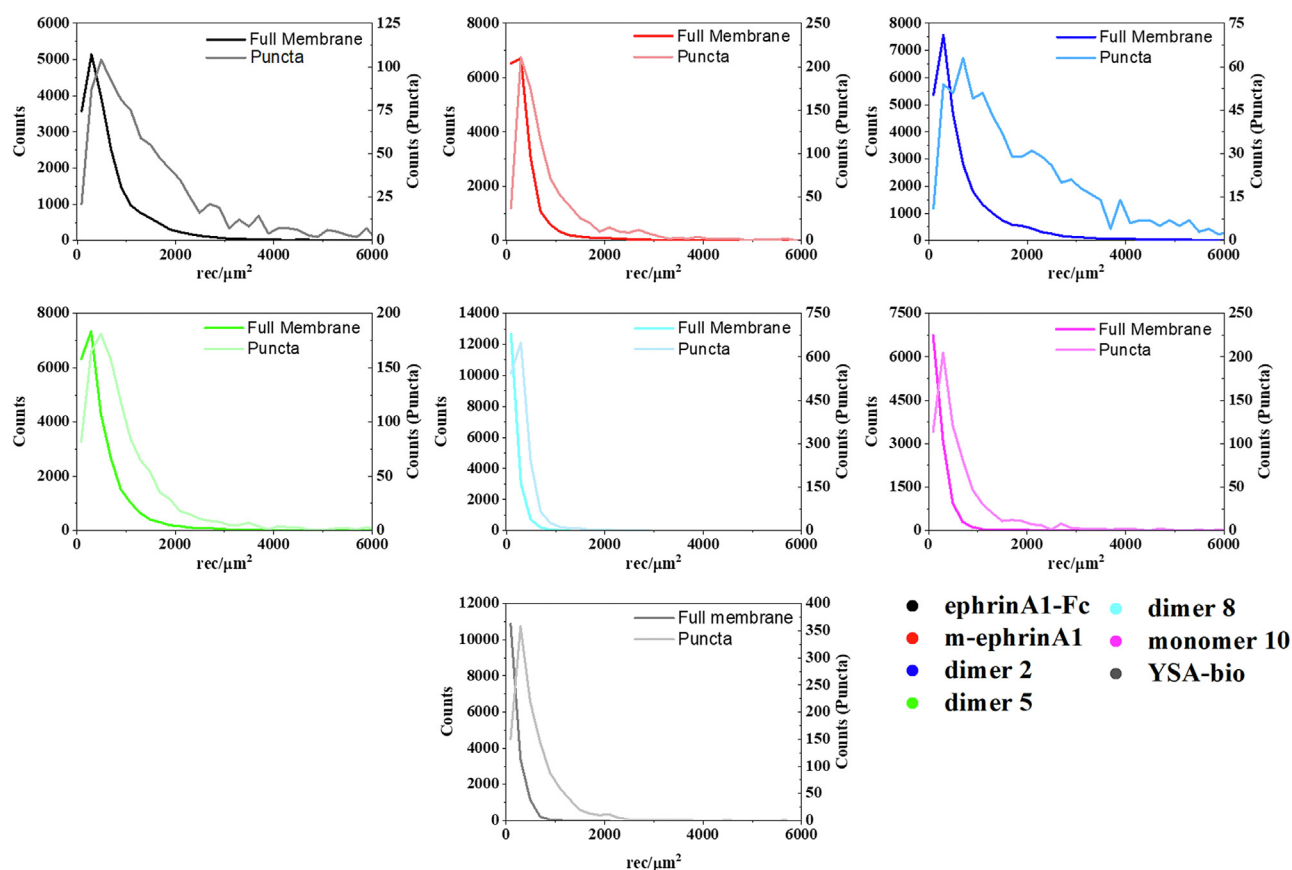


Figure 5. Comparison of the frequency of occurrence (counts) of EphA2-eYFP concentrations for the whole membrane (left y-axis) and the high-intensity puncta (right y-axis). The counts derived from the puncta are shifted to higher receptor concentration values. eYFP, enhanced YFP.

Only a small fraction of the pixels were removed for puncta analysis, as shown in Figure 4A and indicated in Figure 5 by the different values of the left y-axis (referring to whole membranes) and the right y-axis (referring to the puncta). To directly compare the puncta brightness distributions to the whole membrane brightness distributions, we plotted them side by side while again using two different y-axis scales (Fig. 6). The molecular brightness values for the puncta are shifted to the right, indicating an enrichment of high-order oligomers in the puncta. Indeed, comparison of the mean, median, and mode values derived from analyses of the puncta (Table S2 with those for whole membranes; Table 2) reveals a large increase in the mode of the brightness distributions in the puncta. Curiously, the rank order of peptide mean brightness is different for puncta and whole membranes (Table S4). For example, the mean brightness ranking for dimer 8 is lower in the puncta than in the whole membrane.

Statistical analysis of the correlations between EphA2 signaling characteristics and the mean, median, and mode of the FIF brightness distributions in the puncta did not reveal any correlations (Figs. 7, S3, S4, and Table S3). Thus, a correlation between pY588 efficacy and mean brightness was not observed for the puncta. This lack of correlation may be explained by the fact that EphA2 signaling properties were measured using Western blotting and thus represent mean values in the whole membrane.

Discussion

Here, we demonstrate that FIF spectrometry can be used to study the association of EphA2 into dimers and high-order oligomers in response to different ligands. EphA2 belongs to the RTK family, and thus its function is controlled *via* its oligomerization in the membrane. The formation of RTK dimers, at a minimum, is required for RTK activity, as dimerization brings two kinase molecules in close proximity so they can phosphorylate each other. Furthermore, it is known that the Eph receptors can form high-order oligomers, similar to many other RTKs under certain conditions (59). Although all ligands examined strongly induce EphA2 tyrosine phosphorylation and activation, with the exception of nonbiotinylated YSA, FIF experiments revealed that these ligands induce distinct brightness distributions for EphA2 in both whole membranes and in puncta.

We found that ligands that promote different arrangements of the EphA2 extracellular region can induce puncta with distinct appearance and different receptor oligomerization states, which might be responsible for distinct signaling properties (40). The YSA peptide is the only one of the ligands we examined that does not bridge two EphA2 ligand-binding domains (40). Our FIF experiments substantiate previous FRET experiments showing that YSA promotes the assembly of EphA2 dimers but not high-order oligomers (37, 60), although the underlying mechanism remains unknown.

EphA2 phosphorylation correlates with EphA2 oligomer size

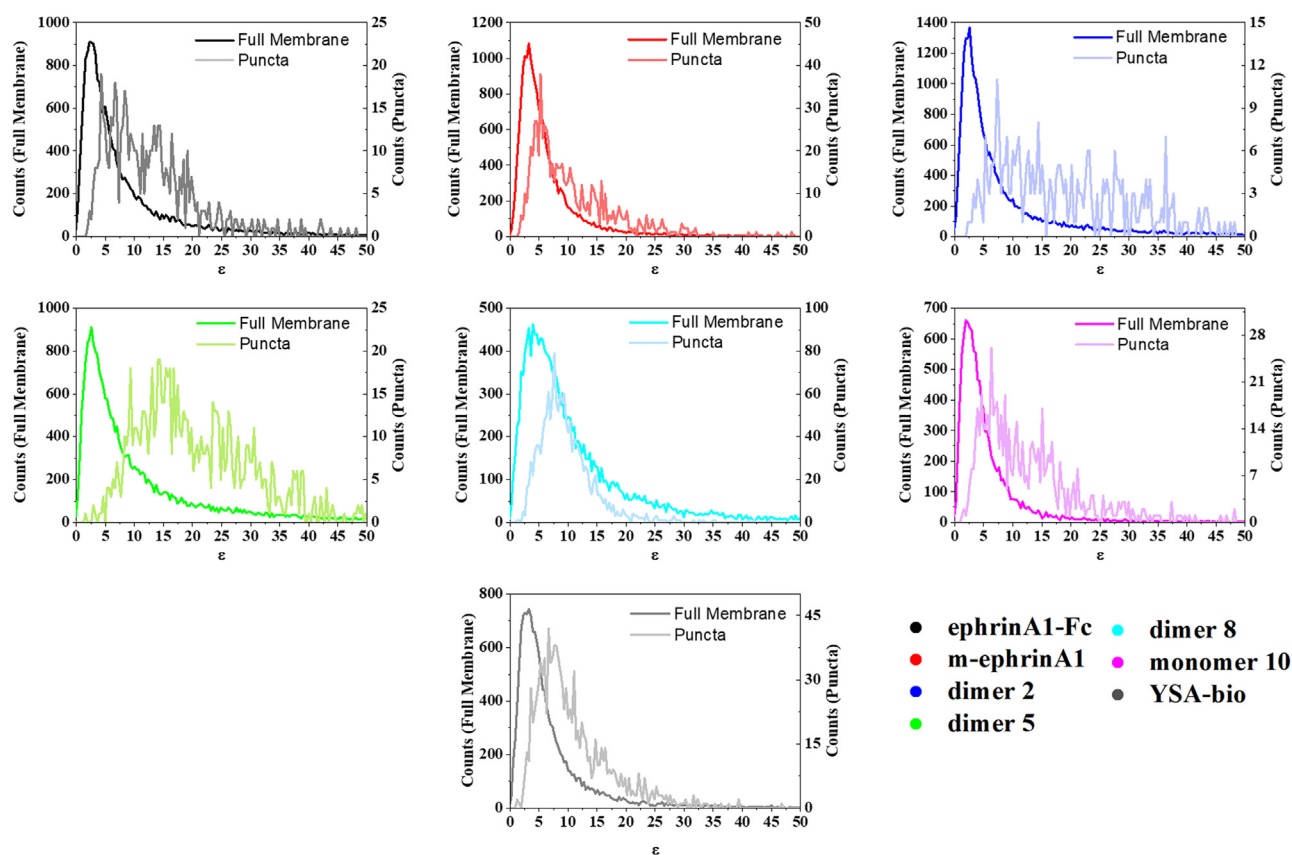


Figure 6. Comparison of molecular brightness distributions for the whole membrane and the puncta. The left y-axis refers to the brightness distributions calculated for the whole membrane. The right y-axis refers to the brightness distribution calculated for the puncta. The distributions derived from the puncta are shifted to higher brightness values.

Interestingly, YSA-induced dimerization occurs with only a small increase in receptor autophosphorylation (40), which conforms well with the correlation we have established between EphA2 Y588 phosphorylation and oligomer size (Fig. 3B).

The fitting of the FIF distributions with log-normal functions revealed a large difference in the mode (the most frequent value) of the distributions, when comparing whole membranes to puncta (compare Tables 2 and S2). The increase in the mode ranged from twofold for m-ephrinA1 and monomer 10 to 6-fold for dimer 5. Thus, the most common oligomer size is higher in the puncta for all ligands. We further found that the mean/median brightness rank order is different for whole membranes and puncta, which may be due to the different appearance of the puncta induced by the various ligands, leading to different efficiencies of pixel identification in the FIF analysis. Only a small fraction of the puncta present in the membrane were identified by the SLIC protocol and used for puncta analyses, perhaps because of the modest (approximately three times) EphA2 enrichment observed in the puncta. Yet, the identified puncta are representative of all puncta, and their analysis gives insight into how oligomer size distributions differ inside and outside the puncta.

An RTK may be activated by different ligands, and there is great interest in developing novel biased ligands that can preferentially modulate a subset of downstream signaling

responses linked to pathogenic signaling. In previous work, we analyzed dose–response curves for different EphA2 ligands to assess bias (40). We compared two well-known EphA2 signaling responses, autophosphorylation on Y588 and downstream inhibition of AKT, in PC3 prostate cancer cells stimulated with different ligands. The bias factor, β_{lig} , revealed that all the peptide ligands and m-ephrin-A1 are significantly biased toward AKT inhibition when compared with ephrin-A1 Fc. In addition, we found that the factors used to calculate β_{lig} , including the efficacy and potency of the responses, differ among the ligands (40). To determine if a correlation exists between β_{lig} efficacies and/or potencies and the size of EphA2 oligomers, we compared these EphA2 signaling parameters previously measured in PC3 prostate cancer cells (which have high expression of endogenous EphA2 (40)) with brightness distributions measured by FIF in HEK293T cells (in which we transiently expressed EphA2 labeled with eYFP). Different responses to ligands can be acquired in different cell lines, as long as each response (in this case, phosphorylation and oligomerization) is measured for all ligands under the same conditions (61–63). This practice is common in studies of G protein–coupled receptors (61), and we use it here for EphA2 as well. Our results in Figures 3, S1, and S2 show no correlation between bias coefficients for EphA2 and the parameters of the EphA2 brightness distributions, measured by FIF.

EphA2 phosphorylation correlates with EphA2 oligomer size

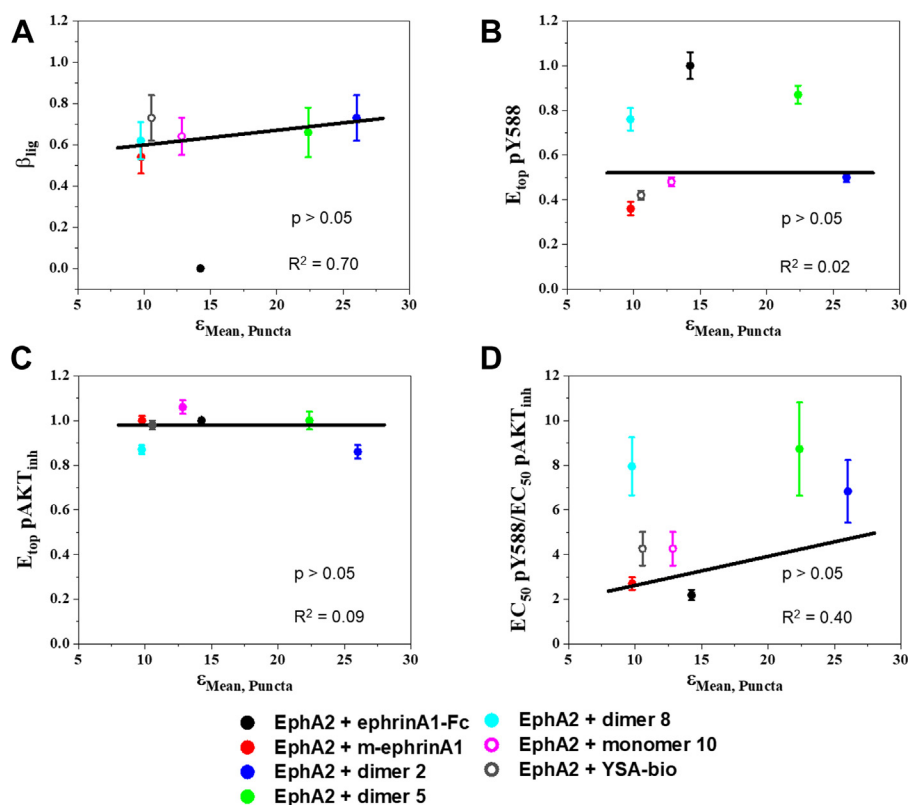


Figure 7. Correlation between EphA2 signaling parameters and the means of the molecular brightness log-normal distributions obtained for the high-intensity puncta. A, ligand bias coefficients *versus* means, when ephrinA1-Fc was used as the reference ligand. B, ligand-specific EphA2 Y588 phosphorylation efficacies, normalized to the value obtained with the reference ligand ephrinA1-Fc, *versus* the means. C, ligand-specific AKT inhibition efficacies, normalized to the value obtained with the reference ligand ephrinA1-Fc, *versus* means. D, ligand-specific ratios of Y588 phosphorylation to AKT inhibition potencies *versus* means. Data points: averages and standard errors from Ref. (40). Lines: linear fits, excluding ephrinA1-Fc.

Although bias coefficients are not different for the peptides and m-ephrinA1, there are quantitative differences in the features of EphA2 signaling used to calculate bias. For instance, the efficacies of the responses induced by the different ligands are significantly different from each other (40). The efficacy is the highest possible response that can be induced by a ligand, typically at high (saturating) ligand concentrations. Here, we find a significant positive correlation between the efficacy of EphA2 Y588 phosphorylation in response to m-ephrinA1 and peptide ligands and the oligomer size. While this correlation does not demonstrate causation, our findings hint at the possibility that the efficacy of EphA2 autophosphorylation may be modulated by agents that control oligomer size. This finding sets the stage for further investigations in different cell lines to assess the general validity of our conclusions. It will be also interesting to investigate whether correlations between autophosphorylation and oligomer size exist for other Eph receptors and other RTKs in general.

Experimental procedures

Plasmids

The EphA2-eYFP complementary DNA was cloned into the pcDNA3.1 (+) mammalian expression vector (37). The eYFP fluorescent protein was attached to the C terminus of EphA2 *via* a flexible 15 amino acid (GGG)₅ linker.

Cell culture

HEK293T cells were cultured in Dulbecco's modified Eagle's medium, supplemented with 10% fetal bovine serum (Thermo Fisher Scientific), 1.8 g/l D-glucose, and 1.5 g/l sodium bicarbonate. Cells were seeded in 35-mm glass-bottom collagen-coated dishes (MatTek's Corporation) at a density of 2.0×10^4 and kept in an incubator at 37 °C with 5% carbon dioxide.

Transfection

Cells were transfected with varying amounts of DNA using Lipofectamine 3000 (Invitrogen) according to the manufacturer's recommended protocol. About 12 h after transfection, the cells were rinsed and starved for 12 h in phenol red-free and serum-free medium containing 0.1% w/v bovine serum albumin.

Imaging

The membranes of cells transfected with EphA2-eYFP were imaged on a Leica SP8 confocal microscope using a photon-counting detector. eYFP was excited using a 488 nm diode laser at 0.1% to avoid photobleaching, at a scanning speed of 20 Hz. Cells were subjected to osmotic stress with a hypo-osmotic medium of 25% starvation medium and 75% water. The swelling induced by the hypo-osmotic medium minimizes the effect of ruffles, folds, invaginations, and other

EphA2 phosphorylation correlates with EphA2 oligomer size

irregularities in the plasma membrane, while also preventing EphA2 endocytosis induced by ligands (64).

About 100 to 150 images were collected for each ligand, containing a total of 200 to 300 cells. One ROI per cell was selected (Fig. 1A), which was divided into segments of 15×15 (225 pixels) as described (8), yielding a total of $\sim 10,000$ to 20,000 segments per dataset for each ligand. Histograms of pixel intensities were constructed for each segment and fitted with a Gaussian function, yielding two parameters: $\langle I_{\text{segment}} \rangle$, the center of the Gaussian, and σ_{segment} , the width of the Gaussian.

The molecular brightness of each segment $\epsilon_{\text{segment}}$ was calculated from:

$$\epsilon_{\text{segment}} = \frac{1}{\gamma} \left(\frac{\sigma_{\text{segment}}^2}{I_{\text{segment}}} - 1 \right) \quad (1)$$

where γ is the shape factor that takes into account the beam intensity shape and the orientation of the sample relative to the beam propagation direction. Here, we use a γ value of 0.5 in all cases (8). The brightness values from thousands of segments were binned and assembled into histograms. The process of fluorescence image analysis, including ROI drawing and segmentation, concentration, and brightness calculation, and further analysis was performed using a computer program described (65).

The brightness distributions were fitted using OriginLab (OriginLab Corp) with a log-normal function given by:

$$y = \frac{A}{\sigma x \sqrt{2\pi}} \exp \left\{ -\frac{[\ln(x) - \mu]^2}{2\sigma^2} \right\} \quad (2)$$

where μ is the mean of the $\ln(x)$ Gaussian distribution and σ is the width of the distribution. These two parameters were used to calculate the mean, median, and mode of the log-normal distributions according to:

$$\text{Mean} = \exp \left(\mu + \left(\frac{\sigma^2}{2} \right) \right) \quad (3)$$

$$\text{Median} = \exp(\mu) \quad (4)$$

$$\text{Mode} = \exp(\mu - \sigma^2) \quad (5)$$

Note that the mean, median, and mode are the same for a normal distribution but are different for a log-normal distribution. The errors of composite values were determined using error propagation algorithms (66). To compare brightness distributions, the curves were integrated using Origin Lab (<https://www.originlab.com/>), and the calculated areas were used to normalize distributions such that they have the same area.

Correlations

GraphPad Prism 8.3 (GraphPad Software, Inc) was used to assess the correlations between (i) previously reported EphA2

ligand bias coefficients, efficacies, and potency ratios (40) and (ii) the mean, median, and mode of the molecular brightness distributions obtained from FIF. The mean, median, or mode was set as the independent variable (X), whereas the ligand bias coefficients, efficacies, or potency ratios were set as the dependent variable (Y). The data were fit to a linear function with the dependent variables weighted by $\frac{1}{(\text{SD})^2}$, where the SD was determined from the values of SE and the total number of samples, given by the number of biological repeats N reported (40) times the different ligand concentrations used in the experiments. The slopes determined in the fits (reported in Tables S1 and S3) were compared with the null hypothesis of zero slope using a one-sample *t* test. $p = 0.05$ was the cutoff for the significance of the correlations.

Puncta identification and analysis

Most fluorescence images of cells treated with EphA2 ligands exhibited an abundance of puncta (or “spots”), that is, small groups of pixels with average intensities significantly higher than the surrounding membrane regions. The puncta were identified and separated for further analysis as discussed (9). Briefly, image ROIs were subjected to an SLIC algorithm that identifies the puncta and separates them from the cell membrane images (9). SLIC is an iterative algorithm that assigns each pixel to a certain ROI segment by calculating its “distance” to the closest segment center (67). The distance incorporates the difference between the coordinates of the pixel and the segment center as well as the difference between the fluorescence intensities of the pixels at the two coordinates. The process is terminated when either the number of iterations reaches a chosen maximum value or the shape of the segments surrounding a punctum and the positions of the segments’ centers no longer change significantly. Full details regarding the application of SLIC to the identification of image puncta in fluorescence micrographs and subsequent analysis are provided in a recent publication (9). The entire protocol for puncta identification and analysis is incorporated into the program described (65). Practically, the process is started by segmenting an ROI using an initial segment size of 7×7 , and the SLIC algorithm modifies the specific borders of the segments so that puncta of size commensurate with that of the initial segment are identified. For brightness analysis, the pixels of at least four puncta with similar average intensity are combined into clusters, yielding single molecular brightness values for each cluster. Brightness values derived from the clusters of puncta are then histogrammed and analyzed in a manner similar to those of whole membranes.

Data availability

All data are included in the article.

Supporting information—This article contains supporting information.

Author contributions—E. B. P. and K. H. conceptualization; V. R. methodology; G. B. software; E. Z.-M. and W. C. W. formal analysis;

E. Z.-M. and D. M. investigation; E. Z.-M. writing—original draft; W. C. W., E. B. P., V. R., and K. H. writing—review & editing; V. R. and K. H. supervision; E. B. P. and K. H. funding acquisition.

Funding and additional information—Supported by the National Institutes of Health grants R01GM131374 (to E. B. P. and K. H.), R01GM068619 (to K. H.), and R21AI154284 (to W. W.), National Science Foundation grants MCB 2106031 (to K. H.) and DBI 1919670 (to V. R.), and the University of Wisconsin—Milwaukee RGI grant 101X396 (to V. R.). The content is solely the responsibility of the authors and does not necessarily represent the official views of the National Institutes of Health.

Conflict of interest—The authors declare that they have no conflicts of interest with the contents of this article.

Abbreviations—The abbreviations used are: eYFP, enhanced YFP; FCCS, fluorescence cross-correlation spectroscopy; FIF, fluorescence intensity fluctuation; HEK293T, human embryonic kidney 293T cell line; m-ephrinA1, monomeric soluble form of the ephrinA1 ligand; N&B, number and brightness; NGF, nerve growth factor; ROI, region of interest; RTK, receptor tyrosine kinase; SLIC, simple linear iterative clustering; SPIDA, spatial intensity distribution analysis.

References

1. Kozer, N., Henderson, C., Jackson, J. T., Nice, E. C., Burgess, A. W., and Clayton, A. H. A. (2011) Evidence for extended YFP-EGFR dimers in the absence of ligand on the surface of living cells. *Phys. Biol.* **8**, 066002
2. Wallrabe, H., and Periasamy, A. (2005) Imaging protein molecules using FRET and FLIM microscopy. *Curr. Opin. Biotechnol.* **16**, 19–27
3. Wouters, F. S., and Bastiaens, P. I. (1999) Fluorescence lifetime imaging of receptor tyrosine kinase activity in cells. *Curr. Biol.* **9**, 1127–1130
4. King, C., Stoneman, M., Raicu, V., and Hristova, K. (2016) Fully quantified spectral imaging reveals *in vivo* membrane protein interactions. *Integr. Biol.(Camb.)* **8**, 216–229
5. Sarabipour, S., Del Piccolo, N., and Hristova, K. (2015) Characterization of membrane protein interactions in plasma membrane derived vesicles with quantitative imaging forster resonance energy transfer. *Acc. Chem. Res.* **48**, 2262–2269
6. Paul, M. D., Grubb, H. N., and Hristova, K. (2020) Quantifying the strength of heterointeractions among receptor tyrosine kinases from different subfamilies: implications for cell signaling. *J. Biol. Chem.* **295**, 9917–9933
7. Stoneman, M. R., Raicu, N., Biener, G., and Raicu, V. (2020) Fluorescence-based methods for the study of protein-protein interactions modulated by ligand binding. *Curr. Pharm. Des.* **26**, 5668–5683
8. Stoneman, M. R., Biener, G., Ward, R. J., Pediani, J. D., Badu, D., Eis, A., *et al.* (2019) A general method to quantify ligand-driven oligomerization from fluorescence-based images. *Nat. Met.* **16**, 493–496
9. Biener, G., Stoneman, M. R., and Raicu, V. (2021) Fluorescence intensity fluctuation analysis of receptor oligomerization in membrane domains. *Biophys. J.* **120**, 3028–3039
10. Digman, M. A., Sengupta, P., Wiseman, P. W., Brown, C. M., Horwitz, A. R., and Gratton, E. (2005) Fluctuation correlation spectroscopy with a laser-scanning microscope: exploiting the hidden time structure. *Biophys. J.* **88**, L33–36
11. Hendrix, J., and Lamb, D. C. (2014) Implementation and application of pulsed interleaved excitation for dual-color FCS and RICS. *Met. Mol. Biol.* **1076**, 653–682
12. Christie, S., Shi, X., and Smith, A. W. (2020) Resolving membrane protein-protein interactions in live cells with pulsed interleaved excitation fluorescence cross-correlation spectroscopy. *Acc. Chem. Res.* **53**, 792–799
13. Huang, Y., Bharill, S., Karandur, D., Peterson, S. M., Marita, M., Shi, X., *et al.* (2016) Molecular basis for multimerization in the activation of the epidermal growth factor receptor. *Life* **5**
14. Shi, X., Hapiak, V., Zheng, J., Muller-Greven, J., Bowman, D., Lingerak, R., *et al.* (2017) A role of the SAM domain in EphA2 receptor activation. *Sci. Rep.* **7**, 45084
15. Digman, M. A., Dalal, R., Horwitz, A. F., and Gratton, E. (2008) Mapping the number of molecules and brightness in the laser scanning microscope. *Biophys. J.* **94**, 2320–2332
16. Nagy, P., Claus, J., Jovin, T. M., and Arndt-Jovin, D. J. (2010) Distribution of resting and ligand-bound ErbB1 and ErbB2 receptor tyrosine kinases in living cells using number and brightness analysis. *Proc. Natl. Acad. Sci. U. S. A.* **107**, 16524–16529
17. Paul, M. D., Rainwater, R., Zuo, Y., Gu, L., and Hristova, K. (2021) Probing membrane protein association using concentration-dependent number and brightness. *Angew. Chem. Int. Ed. Engl.* **60**, 6503–6508
18. Godin, A. G., Costantino, S., Lorenzo, L.-E., Swift, J. L., Sergeev, M., Ribeiro-da-Silva, A., *et al.* (2011) Revealing protein oligomerization and densities *in situ* using spatial intensity distribution analysis. *Proc. Natl. Acad. Sci. U. S. A.* **108**, 7010–7015
19. Pasquale, E. B. (2010) Eph receptors and ephrins in cancer: bidirectional signalling and beyond. *Nat. Rev. Cancer* **10**, 165–180
20. Barquilla, A., and Pasquale, E. B. (2015) Eph receptors and ephrins: therapeutic opportunities. *Annu. Rev. Pharmacol. Toxicol.* **55**, 465–487
21. Wilson, K., Shiu, E., and Brantley-Sieders, D. M. (2021) Oncogenic functions and therapeutic targeting of EphA2 in cancer. *Oncogene* **40**, 2483–2495
22. Pandey, A., Shao, H., Marks, R. M., Polverini, P. J., and Dixit, V. M. (1995) Role of B61, the ligand for the Eck receptor tyrosine kinase, in TNF-alpha-induced angiogenesis. *Science* **268**, 567–569
23. Ogawa, K., Pasqualini, R., Lindberg, R. A., Kain, R., Freeman, A. L., and Pasquale, E. B. (2000) The ephrin-A1 ligand and its receptor, EphA2, are expressed during tumor neovascularization. *Oncogene* **19**, 6043–6052
24. Cheng, N., Brantley, D. M., Liu, H., Lin, Q., Enriquez, M., Gale, N., *et al.* (2002) Blockade of EphA receptor tyrosine kinase activation inhibits vascular endothelial cell growth factor-induced angiogenesis. *Mol. Cancer Res.* **1**, 2–11
25. Brantley-Sieders, D. M., Caughron, J., Hicks, D., Pozzi, A., Ruiz, J. C., and Chen, J. (2004) EphA2 receptor tyrosine kinase regulates endothelial cell migration and vascular assembly through phosphoinositide 3-kinase-mediated Rac1 GTPase activation. *J. Cell Sci.* **117**, 2037–2049
26. Zhou, N., Zhao, W. D., Liu, D. X., Liang, Y., Fang, W. G., Li, B., *et al.* (2011) Inactivation of EphA2 promotes tight junction formation and impairs angiogenesis in brain endothelial cells. *Microvasc. Res.* **82**, 113–121
27. Coulthard, M. G., Morgan, M., Woodruff, T. M., Arumugam, T. V., Taylor, S. M., Carpenter, T. C., *et al.* (2012) Eph/Ephrin signaling in injury and inflammation. *Am. J. Pathol.* **181**, 1493–1503
28. Funk, S. D., and Orr, A. W. (2013) Ephs and ephrins resurface in inflammation, immunity, and atherosclerosis. *Pharmacol. Res.* **67**, 42–52
29. Finney, A. C., Funk, S. D., Green, J. M., Yurdagul, A., Jr., Rana, M. A., Pistorius, R., *et al.* (2017) EphA2 expression regulates inflammation and fibroproliferative remodeling in atherosclerosis. *Circulation* **136**, 566–582
30. Shiels, A., Bennett, T. M., Knopf, H. L., Maraini, G., Li, A., Jiao, X., *et al.* (2008) The EPHA2 gene is associated with cataracts linked to chromosome 1p. *Mol. Vis.* **14**, 2042–2055
31. Zhang, T., Hua, R., Xiao, W., Burdon, K. P., Bhattacharya, S. S., Craig, J. E., *et al.* (2009) Mutations of the EPHA2 receptor tyrosine kinase gene cause autosomal dominant congenital cataract. *Hum. Mutat.* **30**, E603–611
32. Park, J. E., Son, A. I., Hua, R., Wang, L., Zhang, X., and Zhou, R. (2012) Human cataract mutations in EPHA2 SAM domain alter receptor stability and function. *PLoS One* **7**, e36564
33. Cheng, C., Ansari, M. M., Cooper, J. A., and Gong, X. (2013) EphA2 and Src regulate equatorial cell morphogenesis during lens development. *Development* **140**, 4237–4245

EphA2 phosphorylation correlates with EphA2 oligomer size

34. Gordon, K., Kochkodan, J. J., Blatt, H., Lin, S. Y., Kaplan, N., Johnston, A., *et al.* (2013) Alteration of the EphA2/Ephrin-A signaling axis in psoriatic epidermis. *J. Invest. Dermatol.* **133**, 712–722
35. Gomez-Soler, M., and Pasquale, E. B. (2021) Eph receptors and ephrins. In: Offermanns, S., Rosenthal, W., eds. *Encyclopedia of Molecular Pharmacology*, 3rd Ed., Springer Nature, Switzerland. pp in press
36. Noberini, R., Lamberto, I., and Pasquale, E. B. (2012) Targeting Eph receptors with peptides and small molecules: progress and challenges. *Semin. Cell Dev. Biol.* **23**, 51–57
37. Singh, D. R., Kanvinder, P., King, C., Pasquale, E. B., and Hristova, K. (2018) The EphA2 receptor is activated through induction of distinct, ligand-dependent oligomeric structures. *Commun. Biol.* **1**, 15
38. Himanen, J. P., Yermekbayeva, L., Janes, P. W., Walker, J. R., Xu, K., Atapattu, L., *et al.* (2010) Architecture of Eph receptor clusters. *Proc. Natl. Acad. Sci. U. S. A.* **107**, 10860–10865
39. Seiradake, E., Harlos, K., Sutton, G., Aricescu, A. R., and Jones, E. Y. (2010) An extracellular steric seeding mechanism for Eph-ephrin signaling platform assembly. *Nat. Struct. Mol. Biol.* **17**, 398–402
40. Gomez-Soler, M., Gehring, M. P., Lechtenberg, B. C., Zapata-Mercado, E., Ruelos, A., Matsumoto, M. W., *et al.* (2022) Ligands with different dimeric configurations potentially activate the EphA2 receptor and reveal its potential for biased signaling. *iScience* **25**, 103870
41. Lechtenberg, B. C., Gehring, M. P., Light, T. P., Horne, C. R., Matsumoto, M. W., Hristova, K., *et al.* (2021) Regulation of the EphA2 receptor intracellular region by phosphomimetic negative charges in the kinase-SAM linker. *Nat. Commun.* **12**, 7047
42. Verheyen, T., Fang, T., Lindenhofer, D., Wang, Y., Akopyan, K., Lindqvist, A., *et al.* (2020) Spatial organization-dependent EphA2 transcriptional responses revealed by ligand nanocalipers. *Nucl. Acids Res.* **48**, 5777–5787
43. Xu, Q., Lin, W. C., Petit, R. S., and Groves, J. T. (2011) EphA2 receptor activation by monomeric Ephrin-A1 on supported membranes. *Biophys. J.* **101**, 2731–2739
44. Dugineni, S., Mitra, S., Lamberto, I., Han, X., Xu, Y., An, J., *et al.* (2013) Design and synthesis of potent bivalent peptide agonists targeting the EphA2 receptor. *ACS Med. Chem. Lett.* **4**, 344–348
45. Gomez-Soler, M., Petersen Gehring, M., Lechtenberg, B. C., Zapata-Mercado, E., Hristova, K., and Pasquale, E. B. (2019) Engineering nanomolar peptide ligands that differentially modulate EphA2 receptor signaling. *J. Biol. Chem.* **294**, 8791–8805
46. Lamberto, I., Lechtenberg, B. C., Olson, E. J., Mace, P. D., Dawson, P. E., Riedl, S. J., *et al.* (2014) Development and structural analysis of a nanomolar cyclic peptide antagonist for the EphA4 receptor. *ACS Chem. Biol.* **9**, 2787–2795
47. Gambini, L., Salem, A. F., Udompholkul, P., Tan, X. F., Baggio, C., Shah, N., *et al.* (2018) Structure-based design of novel EphA2 agonistic agents with nanomolar affinity *in vitro* and in cell. *ACS Chem. Biol.* **13**, 2633–2644
48. Salem, A. F., Wang, S., Billet, S., Chen, J. F., Udompholkul, P., Gambini, L., *et al.* (2018) Reduction of circulating cancer cells and metastases in breast-cancer models by a potent EphA2-agonistic peptide-drug conjugate. *J. Med. Chem.* **61**, 2052–2061
49. Mudd, G. E., Brown, A., Chen, L., van Rietschoten, K., Watcham, S., Teufel, D. P., *et al.* (2020) Identification and optimization of EphA2-selective bicycles for the delivery of cytotoxic payloads. *J. Med. Chem.* **63**, 4107–4116
50. Riedl, S. J., and Pasquale, E. B. (2015) Targeting the Eph system with peptides and peptide conjugates. *Curr. Drug Targets* **16**, 1031–1047
51. Miao, H., Li, D. Q., Mukherjee, A., Guo, H., Petty, A., Cutter, J., *et al.* (2009) EphA2 mediates ligand-dependent inhibition and ligand-independent promotion of cell migration and invasion via a reciprocal regulatory loop with akt. *Cancer Cell* **16**, 9–20
52. Yang, N. Y., Fernandez, C., Richter, M., Xiao, Z., Valencia, F., Tice, D. A., *et al.* (2011) Crosstalk of the EphA2 receptor with a serine/threonine phosphatase suppresses the Akt-mTORC1 pathway in cancer cells. *Cell Signal.* **23**, 201–212
53. Singh, D. R., Ahmed, F., Paul, M. D., Gedam, M., Pasquale, E. B., and Hristova, K. (2016) The SAM domain inhibits EphA2 interactions in the plasma membrane. *Biochim. Biophys. Acta* **1864**, 31–38
54. Ahmed, F., Zapata-Mercado, E., Rahman, S., and Hristova, K. (2021) The biased ligands NGF and NT-3 differentially stabilize Trk-A dimers. *Bio-phys. J.* **120**, 55–63
55. Seiradake, E., Schaupp, A., Ruiz, D. D. T., Kaufmann, R., Mitakidis, N., Harlos, K., *et al.* (2013) Structurally encoded intraclass differences in EphA clusters drive distinct cell responses. *Nat. Struct. Mol. Biol.* **20**, 958–964
56. Rajagopal, S., Ahn, S., Rominger, D. H., Gowen-MacDonald, W., Lam, C. M., Dewire, S. M., *et al.* (2011) Quantifying ligand bias at seven-transmembrane receptors. *Mol. Pharmacol.* **80**, 367–377
57. Kenakin, T., Watson, C., Muniz-Medina, V., Christopoulos, A., and Novick, S. (2012) A simple method for quantifying functional selectivity and agonist bias. *ACS Chem. Neurosci.* **3**, 193–203
58. Kenakin, T. (2017) A scale of agonism and allosteric modulation for assessment of selectivity, bias, and receptor mutation. *Mol. Pharmacol.* **92**, 414–424
59. Needham, S. R., Roberts, S. K., Arkhipov, A., Mysore, V. P., Tynan, C. J., Zanetti-Domingues, L. C., *et al.* (2016) EGFR oligomerization organizes kinase-active dimers into competent signalling platforms. *Nat. Commun.* **7**, 13307
60. Singh, D. R., Pasquale, E. B., and Hristova, K. (2016) A small peptide promotes EphA2 kinase-dependent signaling by stabilizing EphA2 dimers. *Biochim. Biophys. Acta* **1860**, 1922–1928
61. Kenakin, T. (2016) Measurement of receptor signaling bias. *Curr. Protoc. Pharmacol.* **74**. <https://doi.org/10.1002/cpph.11>
62. Kenakin, T. (2019) Biased receptor signaling in drug discovery. *Pharmacol. Rev.* **71**, 267–315
63. Kenakin, T. (2017) Signaling bias in drug discovery. *Expert Opin. Drug Discov.* **12**, 321–333
64. Sinha, B., Koster, D., Ruez, R., Gonnord, P., Bastiani, M., Abankwa, D., *et al.* (2011) Cells respond to mechanical stress by rapid disassembly of caveolae. *Cell* **144**, 402–413
65. Killeen, T. D., Rahman, S., Badu, D. N., Biener, G., Stoneman, M. R., and Raicu, V. (2022) Fluorescence intensity fluctuation analysis of protein oligomerization in cell membranes. *Curr. Protoc.* **2**, e384
66. Bevington, P. R. (1969) *Data Reduction and Error Analysis for the Physical Sciences*, McGraw-Hill Book Company, NY
67. Achanta, R., Shaji, A., Smith, K., Lucchi, A., Fua, P., and Susstrunk, S. (2012) SLIC superpixels compared to state-of-the-art superpixel methods. *IEEE Trans. Pattern Anal. Mach. Intell.* **34**, 2274–2282
68. Bartley, T. D., Hunt, R. W., Welcher, A. A., Boyle, W. J., Parker, V. P., Lindberg, R. A., *et al.* (1994) B61 is a ligand for the ECK receptor protein-tyrosine kinase. *Nature* **368**, 558–560